ACS APPLIED MATERIALS & INTERFACES

Research Article

www.acsami.org

Imidazolium-Containing ABA Triblock Copolymers as Electroactive Devices

Evan Margaretta,[†] Gregory B. Fahs,[†] David L. Inglefield, Jr.,[†] Chainika Jangu,[†] Dong Wang,[‡] James R. Heflin,[‡] Robert B. Moore,[†] and Timothy E. Long*[,†]

[†]Department of Chemistry, Macromolecules and Interfaces Institute, and [‡]Department of Physics, Virginia Tech, Blacksburg, Virginia 24061, United States

Supporting Information

ABSTRACT: Two-step reversible addition−fragmentation chain transfer (RAFT) polymerization and two subsequent postpolymerization modification steps afforded well-defined ABA triblock copolymers featuring mechanically reinforcing polystyrene outer blocks and 1-methylimidazole-neutralized poly(acrylic acid)-based central blocks. Size exclusion chromatography and ^{1}H NMR spectroscopy confirmed predictable molecular weights and narrow distributions. The ionic liquid (IL) 1-ethyl-3-methylimidazolium trifluoromethanesulfonate ([EMIm][OTf]) was incorporated at 30 wt % into polymeric films. Thermogravimetric analysis, differential scanning calorimetry, and dynamic mechanical analysis determined the thermomechanical properties of the polymers and polymer−IL composites. Atomic force microscopy, small-angle X-ray scattering (SAXS), and transmission electron microscopy (TEM) determined surface and bulk morphologies, and poly(Sty-*b*-AA(MeIm)-*b*-Sty) exhibited a change from packed cylindrical to lamellar morphology in SAXS upon IL incorporation. Electrochemical impedance spectroscopy determined the in-plane ionic conductivities of the polymer−IL membranes ($\sigma \sim 10^{-4}$ S/cm). A device fabricated from poly(Sty-*b*-AA(MeIm)-*b*-Sty) with 30 wt % incorporated IL demonstrated mechanical actuation under a low applied voltage of 4 V.

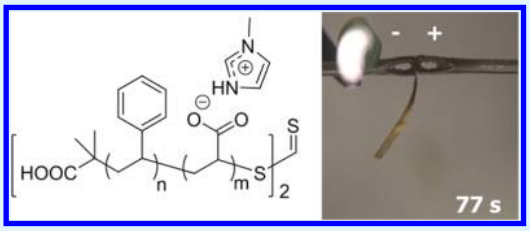

KEYWORDS: *controlled polymerization, block copolymers, ionic liquids, self-assembly, electromechanical actuators*

INTRODUCTION

Polymer−ionic liquid composites represent an emerging field of study owing to their synergy of thermomechanical and conductive properties.[1,2] In particular, polymers in conjunction with ionic liquid (IL) demonstrate suitability for various applications including sensors, artificial muscle, devices for energy harvesting, and gas separation membranes.[3−6] Electromechanical actuators based on IL-containing polymeric membranes offer robust mechanical integrity, greater design versatility, and enhanced response at low applied potential (<10 V).[4,5,7]

The use of block copolymers in ion−polymer transducers offers greater control over actuator properties. Block copolymers offer the advantage of tailored microphase-separated morphology, which greatly affects ionic conductivity in block copolymer films. Mahanthappa et al. showed the change in ionic conductivity as AB diblock copolymer morphology changed from hexagonally packed cylinders to lamellar, and they compared these values to the corresponding homopolymer.[8] Elabd et al. also demonstrated the superior ionic conductivities on the scale of two orders of magnitude for weakly microphase-separated AB diblock copolymers over their random copolymer analogues despite the absence of long-range periodicity.[9]

ABA triblock copolymers exhibit superior mechanical properties over AB diblock copolymers of similar composition, resulting from physical cross-linking on each end of the low-T_g central block. Variation of block length and relative block incorporation enables precise tailoring of thermomechanical, morphological, and conductive properties of the final electromechanical transducer.[7,10,11] For instance, Long et al. recently demonstrated ionic conductivity dependence on relative block lengths for ABA triblock copolymers with charged central blocks.[10] Several studies also report the preferential interaction of IL with polar phases of block copolymer matrices, demonstrating further suitability of block copolymers for electroactive devices.[12−14]

Eisenberg et al. reported extensively on the self-assembling nature of polystyrene (PS) and poly(acrylic acid) (PAA) AB diblock copolymers.[15−19] An additional report studied PS-*b*-PAA-*b*-PS and demonstrated self-assembly in IL 1-butyl-3-methylimidazolium hexafluorophosphate (BMIm PF_6).[20] Transmission electron microscopy (TEM) revealed a change from vesicles to micelles with increased molecular weight of the PAA central block. Another study investigated an AB diblock copolymer of PS and poly(sodium acrylate) (PNaA) in the presence of varying amounts of 1-cetylpyridinium surfactant.[21] In the solid state, these materials contained cetyl chain crystalline domains with amorphous PS and PNaA domains, depending on the level of surfactant loading. Previous work also

Received: October 19, 2015
Accepted: December 23, 2015
Published: December 23, 2015

DOI: 10.1021/acsami.5b09965
ACS Appl. Mater. Interfaces 2016, 8, 1280−1288

established the suitability of imidazolium-containing polymers for electromechanical actuators due to their inherent thermal stability and excellent ionic conductivity.[10,22−24] Vinylbenzylimidazole (VBIm)-based triblock copolymers synthesized with nitroxide-mediated polymerization yielded actuators with response behaviors comparable to industry benchmark Nafion when incorporated with IL.[10] In this case, the imidazolium cation was covalently bound to the polymer backbone. In our other work, alkylimidazole neutralization of a sulfonated symmetric pentablock copolymer and subsequent swelling with IL provided an actuator with a mobile imidazolium counterion.[24]

In the present work, neutralization of PS-*b*-PAA-*b*-PS-based triblock copolymers with 1-methylimidazole (MeIm) presents the imidazolium functionality in novel poly(Sty-*b*-AA(MeIm)-*b*-Sty) and poly(Sty-*b*-[nBA$_{4\%}$-*co*-AA(MeIm)$_{96\%}$]-*b*-Sty) ABA triblock copolymers. This manuscript details the RAFT synthesis and thermomechanical properties of these novel ABA triblock copolymers. Furthermore, the present study examines the incorporation of 1-ethyl-3-methylimidazolium trifluoromethanesulfonate ([EMIm][OTf]) to yield a polymer−IL composite with ionic conductivity on the order of 10^{-4} S/cm and demonstrates actuation behavior of the resulting fabricated electromechanical transducer.

EXPERIMENTAL SECTION

Materials. Styrene (Sty, >99%), *n*-butyl acrylate (nBA, 99%), and *t*-butyl acrylate (tBA, >98%) were purchased from Sigma-Aldrich and passed through a basic alumina column to remove inhibitor. 2,2′-Azobis(isobutyronitrile) (AIBN, Aldrich, 99%) was recrystallized twice from methanol. 1-Methylimidazole (MeIm, ≥99%) was purchased from Sigma-Aldrich and distilled prior to use. 1-Ethyl-3-methylimidazolium trifluoromethanesulfonate ([EMIm][OTf], >99%) was purchased from Sigma-Aldrich and dried *in vacuo* at 100 °C for 18 h prior to use. Carbon disulfide (≥99%), tetrabutyl ammonium hydrogen sulfate (TBA HSO_4, ≥99%), sodium hydroxide (NaOH, ≥97%), anhydrous 1,4-dioxane, HCl (4.0 M in 1,4-dioxane), and phenolphthalein (ACS grade) were purchased from Sigma-Aldrich and used as received. All other solvents were purchased from Spectrum Chemical and used without further purification.

Synthesis of the Polystyrene (PS) Precursor. 2-(1-Carboxy-1-methylsulfanylthiocarbonylsulfanyl)-2-methylpropionic acid (CMP) was synthesized in accordance with previously established literature.[25] In a typical RAFT polymerization, AIBN (16.4 mg, 0.1 mmol), CMP (282 mg, 1 mmol), and Sty (220 mL, 1.92 mol) were added to a 500 mL, round-bottomed flask equipped with magnetic stirring. The solution was sparged with argon for 30 min, and the reaction was subsequently immersed in a mineral oil bath thermostated at 65 °C. Monomer conversion was monitored with ^{1}H NMR spectroscopy in $CDCl_3$ as the reaction proceeded, while THF SEC provided molecular weight data. The reaction was terminated after 48 h at 25% monomer conversion through the introduction of air and removal from heat. To ensure complete monomer removal, the product was precipitated into methanol and collected with vacuum filtration, then subsequently reprecipitated into methanol from a 30 wt % THF solution, collected with vacuum filtration, and dried at 60 °C *in vacuo* for 18 h.

Synthesis of ABA Triblock Copolymers. In a typical RAFT polymerization, a 100 mL, round-bottomed flask equipped with a magnetic stir bar was charged with AIBN (17.6 mg, 107 μmol), PS precursor (10 g, 216 μmol), butyl acrylate (16.6 g, 130 mmol), and *N*,*N*-dimethylformamide (DMF, 64 mL). The relative ratios of tBA and nBA incorporated into the central block of the ABA triblock copolymer were varied, with central block compositions of 0 and 5 mol % nBA targeted. The polymerization reaction was sparged with argon for 20 min to remove air and submerged in a thermostatted 70 °C mineral oil bath. The reaction was terminated after 10 h through the introduction of air and removal from heat. The product was precipitated into a CH_3OH:H_2O mixture (4:1, v:v), and vacuum filtration was employed to collect the solids. ^{1}H NMR spectroscopy provided M_n data for the central block consistent with the molecular weight data as determined through THF SEC and also determined the relative incorporation of tBA and nBA in the central block to be consistent with the charged values. Films of poly(Sty-*b*-tBA-*b*-Sty) and poly(Sty-*b*-[nBA$_{4\%}$-*co*-tBA$_{96\%}$]-*b*-Sty) were cast from 10 wt % in THF. The films were annealed at 110 °C for 8 h and then 110 °C *in vacuo* for 8 h.

Acid Cleavage of *t*-Butyl Esters. *t*-Butyl esters were selectively cleaved through an adapted acidolysis procedure.[26] ABA triblock copolymer was added to a round-bottomed flask equipped with a magnetic stir bar. HCl (4.0 M in 1,4-dioxane) was added to achieve five equivalents of acid per *t*-butyl ester. Additional 1,4-dioxane was added to afford a final polymer concentration of 75 g/L. The reaction flask was sealed and allowed to stir at 25 °C for 48 h. The product was precipitated into hexanes and collected through decantation of the supernatant. The solids were then redissolved in THF at 30 wt % and reprecipitated into hexanes. Vacuum filtration isolated the product, which was washed thoroughly with diethyl ether and collected in quantitative yield. The product was dried at 40 °C *in vacuo* for 18 h. ^{1}H NMR spectroscopy indicated the quantitative selective cleavage of *t*-butyl esters. Films of poly(Sty-*b*-AA-*b*-Sty) and poly(Sty-*b*-[nBA$_{4\%}$-*co*-AA$_{96\%}$]-*b*-Sty) were cast onto Si-coated PET from 10 wt % solutions in 9:2 THF:CH_3OH mixture. The films were dried at 40 °C for 8 h and then at 40 °C *in vacuo* for 8 h.

Neutralization of Carboxylic Acid-Containing Copolymers. To introduce imidazolium groups to the polymer, the acrylic acid units were neutralized with MeIm according to the following procedure. Acid-containing triblock copolymers were dissolved in a round-bottomed flask equipped with a magnetic stir bar at 10 wt % in THF:CH_3OH mixture (9:2, v:v). MeIm was added dropwise in the presence of phenolphthalein indicator until the persistence of a slight pink color, and the solution was allowed to stir for 16 h at 25 °C. The reaction was then dialyzed against THF, and solvent was subsequently removed under rotary evaporation to afford the product in quantitative yield. The product was dried at 40 °C *in vacuo* for 18 h. Films of poly(Sty-*b*-AA(MeIm)-*b*-Sty) and poly(Sty-*b*-[nBA$_{4\%}$-*co*-AA(MeIm)$_{96\%}$]-*b*-Sty) were cast onto Si-coated PET from 10 wt % solutions in THF:CH_3OH mixture (9:2, v:v). The films were further dried at 40 °C for 8 h and then at 40 °C *in vacuo* for 8 h.

Ionic Liquid Incorporation. The ionic liquid (IL) [EMIm][OTf] was incorporated into the imidazolium-containing triblock copolymers in the following fashion. The polymer was dissolved at 10 wt % in THF:CH_3OH mixture (9:2, v:v). [EMIm][OTf] was added by micropipette at 30 wt % IL relative to the polymer. The solution was subjected to magnetic stirring for 24 h at 25 °C. Films were cast directly from solution onto a PTFE substrate and subsequently annealed at 110 °C for 8 h and then at 110 °C *in vacuo* for 8 h. Dried films were stored in a vacuum desiccator until immediately prior to further characterization to eliminate potential water uptake.

Synthesis of Random Copolymer Control. To determine polymer microstructure effect on properties, the random copolymer analogue of poly(Sty-*b*-tBA-*b*-Sty) was synthesized. Sty (5.00 mL, 43.6 mmol), tBA (7.66 mL, 52.3 mmol), AIBN (16.4 mg, 0.1 mmol), and DMF (56.3 mL) were charged to a 100 mL, round-bottomed flask equipped with a magnetic stir bar. The solution was sparged with argon for 20 min and subsequently immersed in a thermostatted 65 °C mineral oil bath and allowed to stir for 24 h. The polymer product was precipitated in 4:1 CH_3OH:H_2O, collected by vacuum filtration, and dried at 50 °C *in vacuo* for 18 h. ^{1}H NMR spectroscopy determined the polymer composition of 61:39 molar ratio of Sty:tBA. THF SEC provided the molecular weight data. Poly(Sty-*co*-tBA) was then subjected to the same acid cleavage and MeIm neutralization modification steps as detailed above. Poly(Sty-*co*-AA(MeIm)) was cast with 30 wt % [EMIm][OTf] from 10 wt % THF solution and annealed for 8 h at 80 °C and then at 80 °C *in vacuo* for an additional 18 h. The dried film was stored in a vacuum desiccator until immediately prior to further characterization to eliminate potential water uptake.

DOI: 10.1021/acsami.5b09965
ACS Appl. Mater. Interfaces 2016, 8, 1280−1288

Scheme 1. Synthesis of (a) Polystyrene Precursor and (b) Poly(styrene-*b*-(*n*BA-*co*-*t*BA)-*b*-styrene) ABA Triblock Copolymer

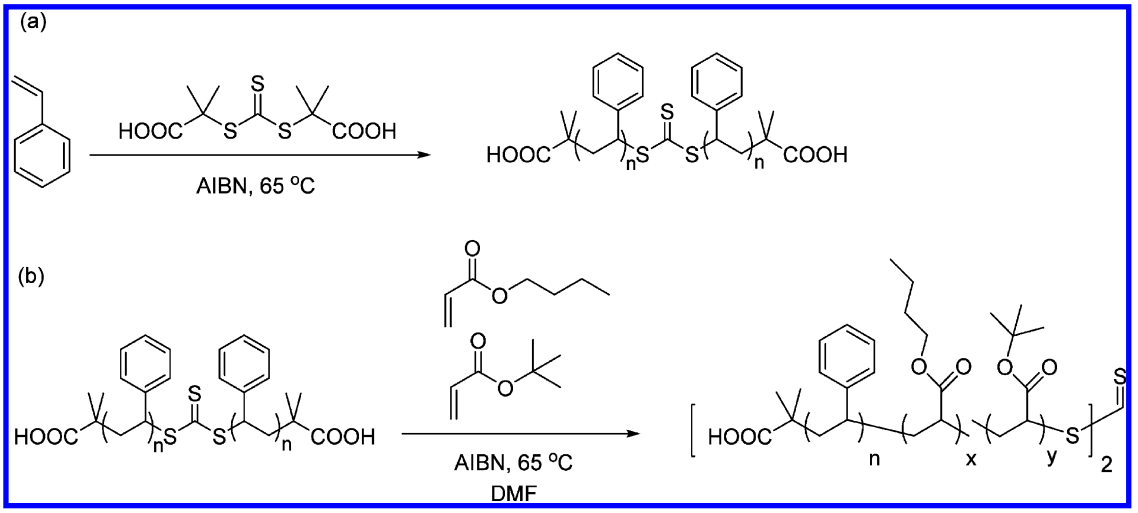

Table 1. Polymer Molecular Weight and Thermal Properties[a]

polymer	M_n (kg/mol)	M_w (kg/mol)	PDI	$T_{g,1}$ (°C)	$T_{g,2}$ (°C)	$T_{d,5\%}$ (°C)
PS precursor	46.4	48.7	1.05	100	--	331
poly(Sty-*b*-tBA-*b*-Sty)	114	136	1.19	101	48	226
poly(Sty-*b*-AA-*b*-Sty)	84.9[b]	101[b]		99	ND	254
poly(Sty-*b*-AA(MeIm)-*b*-Sty)	128[b]	152[b]		98	70	190
with 30 wt % incorporated [EMIm][OTf]				100	8	189
poly(Sty-*b*-[$nBA_{4\%}$-*co*-$tBA_{96\%}$]-*b*-Sty)	119	144	1.21	101	42	231
poly(Sty-*b*-[$nBA_{4\%}$-*co*-$AA_{96\%}$]-*b*-Sty)	88.6[b]	107[b]		100	ND	251
poly(Sty-*b*-[$nBA_{4\%}$-*co*-$AA(MeIm)_{96\%}$]-*b*-Sty)	133[b]	160[b]		100	65	196
with 30 wt % incorporated [EMIm][OTf]				106	−15	192
poly(Sty-*co*-tBA)	78.6	128	1.64	77	--	235
poly(Sty-*co*-AA)	66.1[b]	108[b]		100	--	269
poly(Sty-*co*-AA(MeIm))	119[b]	195[b]		103	--	152
with 30 wt % incorporated [EMIm][OTf]				67	--	201

[a]ND = not determined. [b]Calculated based on quantitative postpolymerization modification steps.

Analytical Methods. ^{1}H NMR spectroscopy (Varian Unity, 400 MHz, $CDCl_3$, DMSO-d_6) confirmed the structure of monomer and polymer in addition to monomer conversion. Melting points were recorded on an Electrothermal 1101D Mel-Temp melting point apparatus operating at 10 °C/min. Tetrahydrofuran (THF) size exclusion chromatography (SEC) at 30 °C using a flow rate of 1.0 mL/min through three Polymer Laboratories PLgel 5 μm MIXED-C columns determined the molecular weights of the obtained polymers. SEC instrumentation included a Waters717plus autosampler equipped with Waters 515 HPLC pump, Waters 2414 refractive index detector, and Wyatt miniDawn MALLS detector operating at 690 nm. Differential scanning calorimetry (DSC, TA Instruments Q2000) determined thermal transitions using a standard heat/cool/heat method with 10 °C/min heating rate and 100 °C/min cooling rate under constant N_2 purge. All glass transition temperature (T_g) values are reported from the second heats. Thermogravimetric analysis (TGA, TA Instruments Q50) recorded the 5% weight loss temperature ($T_{d,5\%}$) of the polymers when subjected to a 10 °C/min temperature ramp under constant N_2 purge. Dynamic mechanical analysis (DMA, TA Instruments Q800) was performed in oscillatory tension mode at 1 Hz with a temperature ramp of 3 °C/min. Electrochemical impedance spectroscopy (EIS, Autolab PGSTAT 302N) was performed using a four-point electrode sample cell at 10% ± 0.1% relative humidity in an ESPEC BTL-433 environmental chamber which controls temperature to 0.1 °C. Alternating sine-wave potential (0.2 V) was applied over a 0.1−10^6 Hz frequency range. The high *x*-axis intercept of the Nyquist plot of imaginary impedance as a function of real impedance gave the resistance value.

Morphological Analysis. A Veeco MultiMode scanning microscope yielded atomic force microscopy (AFM) images. Triblock copolymer films were imaged in tapping mode with a set point ratio of 0.78 using a nanosensor silicon tip with spring constant of 42 N m^{-1}. Samples for transmission electron microscopy were cryomicrotomed, vapor stained for 1 h with OsO_4, and subsequently imaged with a Phillips EM420 transmission electron micrograph operating at 120 kV acceleration voltage. Images were processed with the profile feature in Gatan Digital Micrograph software, and domain sizes are reported as the average of 50 domains from five images of varied magnification.

Small-angle X-ray scattering (SAXS) experiments were performed using a Rigaku S-Max 3000 3 pinhole SAXS system, equipped with a rotating anode emitting X-rays with a wavelength of 0.154 nm (Cu Kα). The sample-to-detector distance was 1603 mm, and q-range was calibrated using a silver behenate standard. Two-dimensional SAXS patterns were obtained using a fully integrated 2D multiwire, proportional counting, gas-filled detector, with an exposure time of 1 h. The SAXS data have been corrected for sample thickness, sample transmission, and background scattering. All the SAXS data were analyzed using the SAXSGUI software package to obtain radially integrated SAXS intensity versus scattering vector q, where $q = (4\pi/\lambda)\sin(\theta)$, θ is one-half of the scattering angle, and λ is the wavelength of X-ray.

Peak positions were determined from an exponential least-squares fit of the 1-D scattering profiles. The fits were performed using a sum of Gaussian distributions. In order to accurately determine the Gaussian fit parameters, a second-order polynomial removed the Bonart thermal background, and Porod's Law accounted for the

DOI: 10.1021/acsami.5b09965
ACS Appl. Mater. Interfaces 2016, 8, 1280−1288

Scheme 2. Postpolymerization Modification (a) of Poly(styrene-*b*-(*n*BA-*co*-*t*BA)-*b*-styrene) to Yield Poly(styrene-*b*-(*n*BA-*co*-AA)-*b*-styrene) and (b) Subsequent Neutralization with 1-Methylimidazole

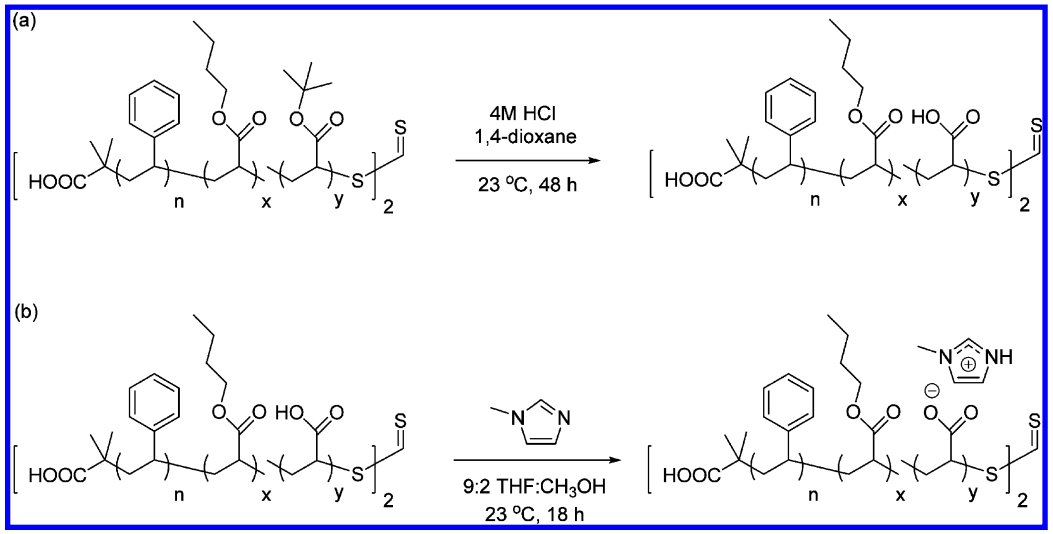

scattering contribution from the phase boundaries. The intensity is defined as follows

$$I(q) = \sum_i G_i(q) + P_2(q) + \frac{K}{q^4}$$

where

$$P_2(q) = a + bq + cq^2 \text{ and } G_i(q) = A_i \exp\left[-\frac{(q - q_{0,i})^2}{2\sigma_i^2}\right]$$

Actuation Behavior. The electromechanical device was fabricated and tested as follows: a gold foil leaf (120 nm thick, L.A. Gold Leaf Wholesaler) electrode was hot pressed on each side of the membrane with 700 lb. force at 90 °C for 20 s. Subsequently the membrane was cut into strips (1 mm by 1 cm) for actuation tests.

The tests were performed on a custom-built probe station which clamps one end of the fabricated device between two electrodes while permitting free movement at the other end. A DC step voltage (4.0 V, HP 6218A power supply) was applied to the actuator. A SONY HXR-MC1 high-definition video camera recorded the bending at 30 FPS for further analysis. The actuation curvature (inverse radius) was determined by the relationships: $I = 2r \sin(\theta/2)$ and $a = r\theta$, where I is the distance between the free tip and the fixed end of the bend actuator, r is the radius of the curve, a is the arc length, and θ is the arc angle. Positive curvature was arbitrarily assigned when the actuator bent toward the cathode, with negative curvature indicating bending toward the anode.

RESULTS AND DISCUSSION

Synthesis and Thermomechanical Characterization. RAFT polymerization afforded precise triblock copolymers using the convergent CTA CMP in two steps (Scheme 1). First, bulk polymerization of styrene yielded the PS precursor used for subsequent central block additions. Then, the controlled central block addition yielded poly(Sty-*b*-tBA-*b*-Sty) and poly(Sty-*b*-[nBA$_{4\%}$-*co*-tBA$_{96\%}$]-*b*-Sty). Table 1 contains the molecular weight data as obtained from THF SEC and ^{1}H NMR spectroscopy and calculated molecular weights of the postmodified polymers (Scheme 2) based on quantitative conversion. The polymer products exhibited no change in molecular weight or PDI in the acid hydrolysis step owing to the chemical stability of the trithiocarbonate functionality under the reaction conditions (Figure S1). Previous literature also established the electrochemical and thermal stability of trithiocarbonate-containing RAFT agents.[27,28] PDI values near 1.2 for the triblocks represented good control for acrylate polymerization given the well-known presence of intra- and intermolecular chain transfer to the acrylic backbone.[29] T_g and $T_{d,5\%}$ values as determined with DSC and TGA, respectively, are reported as well.

TGA (Table 1) data demonstrated clear trends. Degradation of poly(Sty-*b*-tBA-*b*-Sty) and poly(Sty-*b*-[nBA$_{4\%}$-*co*-tBA$_{96\%}$]-*b*-Sty) near 220−230 °C correlated with *t*-butyl ester thermolysis to liberate isobutylene.[30,31] This observed weight loss agreed with incorporation of tBA determined through ^{1}H NMR spectroscopy. Similarly, $T_{d,5\%}$ values observed for poly(Sty-*b*-AA(MeIm)-*b*-Sty) and poly(Sty-*b*-[nBA$_{4\%}$-*co*-AA(MeIm)$_{96\%}$]-*b*-Sty) agreed well with the boiling point of 1-methylimidazole (198 °C), indicating the evolution of 1-methylimidazole following the reverse acid−base reaction.

Observation of two T_gs in DSC (Table 1) indicated the microphase-separated morphology of the triblock copolymers. Copolymerization of nBA and tBA in the central block insertion step yielded a random copolymer central block displaying a T_g at 42 °C, consistent with Fox equation's prediction of 44 °C. Incorporation of nBA imparted greater central block flexibility through decreasing central block T_g. In the case of each triblock copolymer, T_g at or near 100 °C suggested the presence of a PS phase. For poly(Sty-*b*-AA-*b*-Sty) and poly(Sty-*b*-[nBA$_{4\%}$-*co*-AA$_{96\%}$]-*b*-Sty), no second T_g was observed below the $T_{d,5\%}$, likely due to AA dehydration prior to onset of segmental motion. Neutralization to yield poly(Sty-*b*-AA(MeIm)-*b*-Sty) and poly(Sty-*b*-[nBA$_{4\%}$-*co*-AA(MeIm)$_{96\%}$]-*b*-Sty) leads to central block T_g values of 70 and 65 °C, respectively, as a result of decreased hydrogen bonding, suppression of anhydride formation, and increase in free volume concomitant with incorporation of a bulkier MeIm counterion. Upon 30 wt % incorporation of the [EMIm][OTf], the central block T_g values for poly(Sty-*b*-AA(MeIm)-*b*-Sty) and poly(Sty-*b*-[nBA$_{4\%}$-*co*-AA(MeIm)$_{96\%}$]-*b*-Sty) dropped to 8 and −15 °C, respectively. The T_g's of the mechanically reinforcing PS outer blocks remained unchanged, demonstrating selective incorporation of IL to the imidazolium-containing central blocks. The absence of an IL melting endotherm at −13 °C in the DSC thermograms confirmed complete uptake of the

DOI: 10.1021/acsami.5b09965
ACS Appl. Mater. Interfaces 2016, 8, 1280−1288

IL into the polymer and indicated the absence of free IL in the membranes.

The brittle nature of poly(Sty-*b*-AA(MeIm)-*b*-Sty) and poly(Sty-*b*-[nBA$_{4\%}$-*co*-AA(MeIm)$_{96\%}$]-*b*-Sty) prevented determination of thermomechanical properties using DMA. Incorporation of IL through a "cast with" procedure sufficiently plasticized the ion-containing central blocks to yield flexible films suitable for such analysis (Figure 1). DMA demonstrated

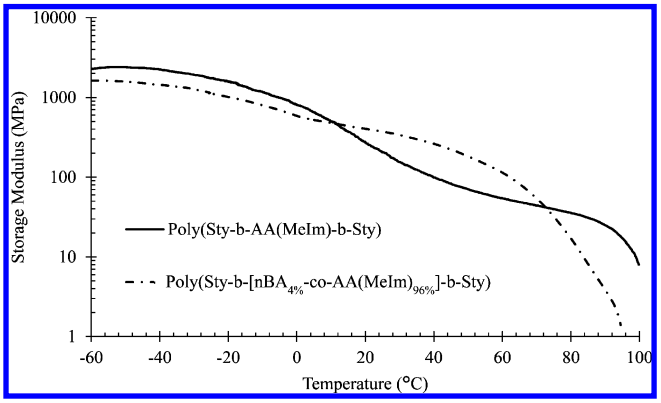

Figure 1. DMA elucidates the thermomechanical properties of the obtained triblock copolymers with 30 wt % incorporated IL.

the microphase separation observed with DSC with two clear transitions evident in each curve. The first decrease in storage moduli occurred at temperatures that corresponded well with central block T_gs, while the flow temperatures near 100 °C related to PS T_g. While the IL-containing membrane of poly(Sty-*b*-[nBA$_{4\%}$-*co*-AA(MeIm)$_{96\%}$]-*b*-Sty) displayed the lower central block T_g in both DMA and DSC, its plateau modulus remained significantly higher than that observed for poly(Sty-*b*-AA(MeIm)-*b*-Sty). A plateau modulus ~100 MPa at room temperature demonstrated the robust mechanical integrity and sufficient flexibility required for electroactive device applications.[22]

Ionic Conductivity. EIS (Figure 2) highlighted the conductive nature of the IL-containing membranes with in-plane ionic conductivities on the order of 10^{-4} S/cm. Poly(Sty-*b*-AA(MeIm)-*b*-Sty) exhibited similar ionic conductivity to poly(Sty-*b*-[nBA$_{4\%}$-*co*-AA(MeIm)$_{96\%}$]-*b*-Sty) over the same temperature range when each membrane possessed 30 wt % [EMIm][OTf]. The brittle nature of the films in the absence of IL prohibited EIS for those samples. When comparing poly(Sty-*b*-AA(MeIm)-*b*-Sty) with its random copolymer analogue poly(Sty-*co*-AA(MeIm)), the importance of microphase-separated morphology was evident, as the random copolymer exhibited conductivities on the order of 10^{-5} S/cm, representing an order of magnitude gain in conductivity upon the introduction of well-defined microphase separation. The increase observed for the in-plane ionic conductivity proves consistent with previous literature observation.[9]

The ionic conductivity values observed here compare well with those previously reported for ionic ABA triblock copolymers as well as fabricated electromechanical devices.[10,22,23] Frisbie and Lodge et al. reported ionic conductivities on the order of 10^{-4} S/cm in the same temperature range for ion gels comprised of 50 wt % PS-*b*-PMMA-*b*-PS (30 wt % PS) in [EMIm][Tf$_2$N].[12] Watanabe then reported the actuation of PS-*b*-PMMA-*b*-PS (48 wt % PS) ion gels comprised of 30 wt % polymer in [EMIm][Tf$_2$N].[13] While Frisbie and Lodge did not

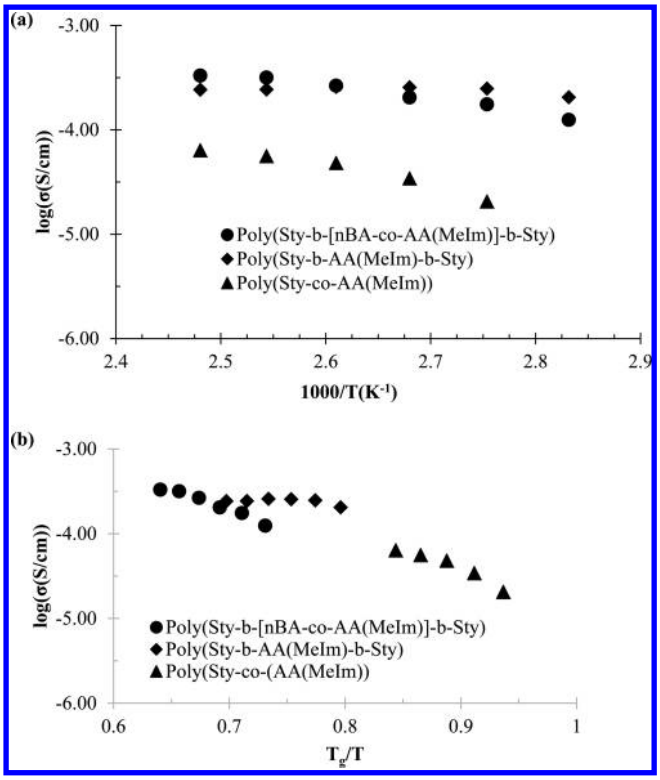

Figure 2. Impedance spectroscopy confirms the superior conductivity in the absence of *n*BA with (a) change in temperature and (b) when normalized by T_g.

comment on the morphology of the ion gels, AFM demonstrated the presence of PS spheres distributed in the IL−PMMA continuous phase in Watanabe's similar ion gels, which also displayed ionic conductivity ~10^{-3} S/cm. The ionic conductivity for poly(Sty-*b*-AA(MeIm)-*b*-Sty) proved within an order of magnitude even at significantly reduced ionic liquid loading, indicating the competitive nature of the polymers with current literature benchmarks, especially given the absence of free IL in the polymer−IL membranes.

Morphological Characterization. AFM (Figure 3a,b) revealed the surface morphologies of poly(Sty-*b*-AA(MeIm)-*b*-Sty) and poly(Sty-*b*-[nBA$_{4\%}$-*co*-AA(MeIm)$_{96\%}$]-*b*-Sty) in the absence of IL and confirmed the phase-separated nature of the materials suggested with DSC. Poly(Sty-*b*-AA(MeIm)-*b*-Sty) exhibits hexagonally packed cylinders on the surface of the membrane, and poly(Sty-*b*-[nBA$_{4\%}$-*co*-AA(MeIm)$_{96\%}$]-*b*-Sty) displays well-defined lamellar surface morphology. In particular, SAXS (Figure 3c, Table 2) indicated the presence of an ordered morphology, consistent with packed cylinders rather than spheres in poly(Sty-*b*-AA(MeIm)-*b*-Sty), with broad scattering peaks at q^*:$\sqrt{3}$:3 The SAXS profile of poly(Sty-*b*-[nBA$_{4\%}$-*co*-AA(MeIm)$_{96\%}$]-*b*-Sty) illustrates the presence of reflections indicative of microphase separation, but in contrast with the AFM results (Figure 3b) it does not conclusively reveal any long-range order in the bulk. Because central block molecular weights remained similar, nBA incorporation into the central block likely affected the Flory−Huggins interaction parameter χ sufficiently enough to induce significant change in morphology. However, the present investigation did not include determination of this parameter.

SAXS also probed bulk morphology of IL-containing membranes (Figure 4), further confirming the phase separation

DOI: 10.1021/acsami.5b09965
ACS Appl. Mater. Interfaces 2016, 8, 1280−1288

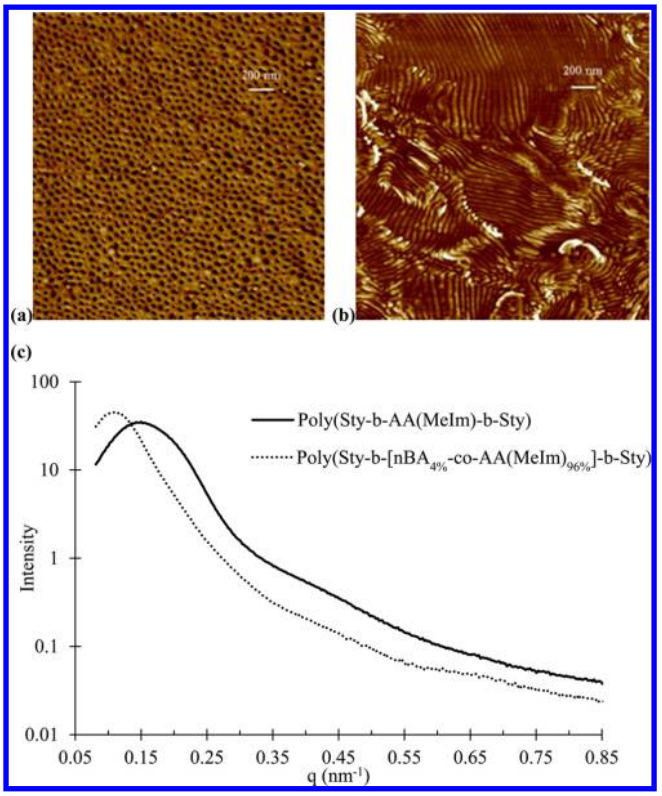

Figure 3. AFM phase images of (a) poly(Sty-*b*-AA(MeIm)-*b*-Sty) and (b) poly(Sty-*b*-[nBA$_{4\%}$-*co*-AA(MeIm)$_{96\%}$]-*b*-Sty) reveal differences in surface morphologies, and (c) SAXS profiles indicate bulk morphologies similar to those observed in AFM.

Table 2. Summary of SAXS Analysis[a]

sample	scattering peaks	morphology
poly(Sty-*b*-AA(MeIm)-*b*-Sty)	q^*, $\sqrt{3}q$, $3q$	cylindrical
with 30 wt % IL	q^*, $3q$, $5q$	lamellar
poly(Sty-*b*-[nBA$_{4\%}$-*co*-AA(MeIm)$_{96\%}$]-*b*-Sty)	q^*	ND
with 30 wt % IL	q^*, $\sqrt{3}q$, $\sqrt{8}q$	ND

[a]ND = not determined.

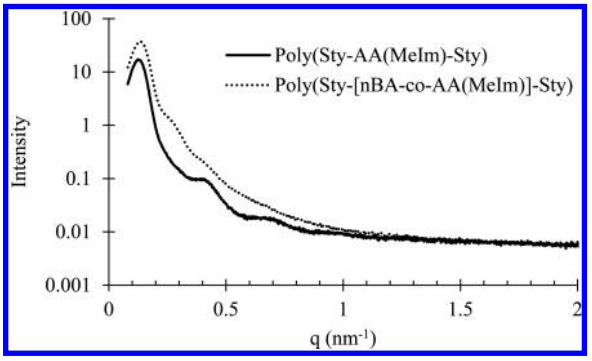

Figure 4. SAXS profiles of poly(Sty-*b*-AA(MeIm)-*b*-Sty) (solid) and poly(Sty-*b*-[nBA$_{4\%}$-*co*-AA(MeIm)$_{96\%}$]-*b*-Sty) (dotted) reveal microphase separation when cast with 30 wt % [EMIm][OTf] ionic liquid.

indicated in DMA and DSC. Scattering peaks at ratios q^*:3:5 suggest lamellar morphology upon the incorporation of IL into poly(Sty-*b*-AA(MeIm)-*b*-Sty) (Table 2). Microphase structure critically affects ionic conductivity of membranes, with films possessing lamellar morphology exhibiting higher ionic conductivity than those having hexagonally packed cylinders.[8] When polymer samples approach 50:50 vol %, structure and form factors in the scattering may overlay and reduce peak intensity at even integral reflections.[32,33] The primary scattering peak position at 0.125 nm^{-1} correlated to *d*-spacing of 50.3 nm. The change from packed cylinders to lamellae ostensibly resulted from varying both χ and volume fraction of the central block. Meanwhile, the SAXS profile for poly(Sty-*b*-[nBA$_{4\%}$-*co*-AA(MeIm)$_{96\%}$]-*b*-Sty) cast with 30 wt % IL indicates microphase-separated bulk morphology with some degree of long-range order; however, the broad secondary scattering peaks of q^*:$\sqrt{3}$:$\sqrt{8}$ do not directly correlate to geometries commonly observed for ABA triblock copolymers.

TEM clearly revealed the bulk morphologies of poly(Sty-*b*-AA(MeIm)-*b*-Sty) and poly(Sty-*b*-[nBA$_{4\%}$-*co*-AA(MeIm)$_{96\%}$]-*b*-Sty), further confirming the SAXS data (Figure 5). The micrographs clearly showed the lamellar bulk morphology of poly(Sty-*b*-AA(MeIm)-*b*-Sty). The images revealed interlamellar spacing of 51.15 ± 4.79 nm, which correlated well with the *d*-spacing as determined using SAXS. Figure 5a demonstrates the small grain size of the lamellar domains, which explains the broad nature of the peaks in the SAXS profiles. Increasing the magnification (Figure 5b) better reveals the well-defined order of the lamellar domains. The small grain size may provide some explanation for the conductivity of the film. Balsara demonstrated the inverse correlation of lamellar domain grain size with ionic conductivity in block copolymer electrolyte samples.[34]

Actuation Behavior. Poly(Sty-*b*-AA(MeIm)-*b*-Sty) proved especially attractive for further investigation of actuation behavior due to its robust thermomechanical properties, superior room-temperature ionic conductivity, and lamellar morphology upon incorporation of IL. The fabricated actuator does not include conductive nanocomposite (CNC) layers between the polymer−IL membrane and the gold electrodes. The layer-by-layer (LbL) assembly process involves repeated sequential immersion of the polymer−IL film into solutions of cationic poly(allyl amine) hydrochloride (PAH) and anionic gold nanoparticles.[10,24] CNC layers impart enhanced ion transport properties and offer increased surface area at the electrode interface.[1,10,22,24] Cationic PAH solution proves sufficiently acidic (pH = 4.0) to protonate the PAA central block (pK_a = 4.7), causing rapid leeching of IL from the membrane, likely a result of MeIm−polymer dissociation in the central block. PAH solutions with pH > 5.0 reduced the rate of—but did not prevent—IL leeching. Therefore, the fabrication process removed CNC LbL assembly in favor of directly hot pressing the gold foil electrodes to each side of the polymer−IL membrane.

Figure 6a illustrates the mechanical deformation response to electric potential stimulus. The membrane initially bent toward the cathode before reversing toward the anode. The bidirectional bending resulted from the time difference between accumulation of mobile cations at the anode and mobile anions at the cathode and typifies polymer−IL transducer actuation.[10,35] These observations proved consistent with Madsen et al.'s diffusion measurements for [EMIm][OTf] in Nafion membranes wherein the larger cation moved up to three times faster at low levels of hydration.[36]

Figure 6b displays the curvature of the device as a function of time during application of electric potential compared to a Nafion control. The actuator exhibited initial forward curvature similar to the previously studied imidazolium sulfonated

DOI: 10.1021/acsami.5b09965
ACS Appl. Mater. Interfaces 2016, 8, 1280−1288

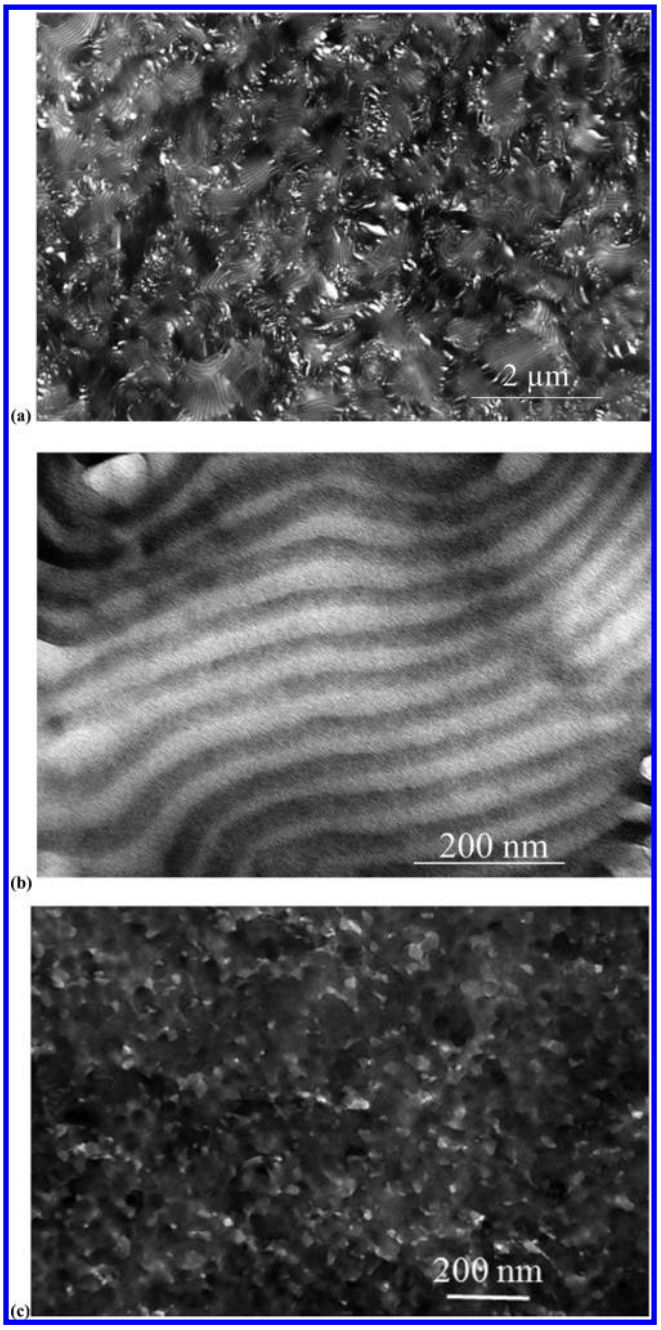

Figure 5. Transmission electron micrographs of OsO_4-stained poly(Sty-*b*-AA(MeIm)-*b*-Sty) at (a) 7500× and (b) 96 000× magnification and (c) poly(Sty-*b*-[$nBA_{4\%}$-*co*-$AA(MeIm)_{96\%}$]-*b*-Sty) at 96 000× magnification. All samples have 30 wt % [EMIm][OTf] incorporated.

pentablock copolymer, although the presently investigated membrane displays a faster response time, even in the absence of CNC layers.[24] The ionic conductivity on the order of 10^{-4} S/cm for poly(Sty-*b*-AA(MeIm)-*b*-Sty) with 30 wt % [EMIm][OTf] as a result of lamellar bulk morphology explains the actuation performance of the fabricated device.

CONCLUSION

For the first time, we prepared an electromechanical transducer using anionic ABA triblock copolymer poly(Sty-*b*-AA(MeIm)-*b*-Sty) and ionic liquid [EMIm][OTf]. RAFT polymerization yielded ABA triblock copolymers poly(Sty-*b*-tBA-*b*-Sty) and

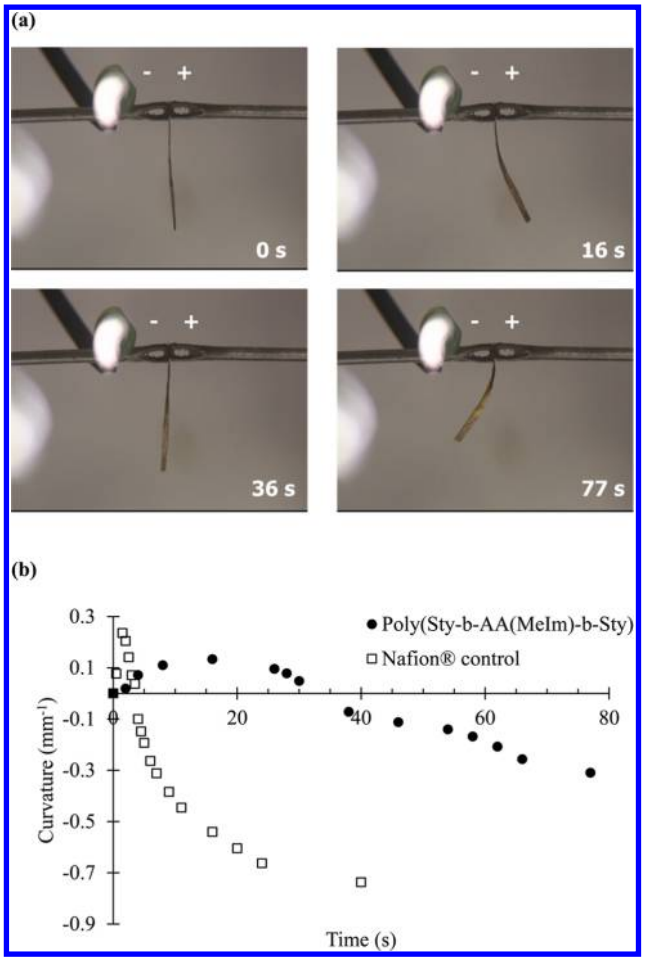

Figure 6. (a) Actuation behavior and (b) curvature of poly(Sty-*b*-AA(MeIm)-*b*-Sty) with 30 wt % EMIm OTf incorporated (●) and Nafion membrane with 29.5 wt % EMIm OTf incorporated (□).

poly(Sty-*b*-[$nBA_{4\%}$-*co*-$tBA_{96\%}$]-*b*-Sty) with PDI of approximately 1.20. Two subsequent postpolymerization modification steps yielded novel ion-containing polymers poly(Sty-*b*-AA(MeIm)-*b*-Sty) and poly(Sty-*b*-[$nBA_{4\%}$-*co*-$AA(MeIm)_{96\%}$]-*b*-Sty). The synthesized polymers exhibited microphase separation as observed using DMA and DSC. SAXS and AFM further confirmed the polymer films' self-assembly. Upon the incorporation of 30 wt % [EMIm][OTf], poly(Sty-*b*-AA(MeIm)-*b*-Sty) demonstrated a plateau modulus ~100 MPa in DMA, desirable for electromechanical transducer fabrication. EIS determined in-plane conductivity values for poly(Sty-*b*-AA(MeIm)-*b*-Sty) and poly(Sty-*b*-[$nBA_{4\%}$-*co*-$AA(MeIm)_{96\%}$]-*b*-Sty) membranes containing 30 wt % IL on the order of 10^{-4} S/cm, representing an order of magnitude increase over a random copolymer analogue. Given the absence of free IL, these conductivity values compete with current literature benchmarks. For the first time, SAXS investigated the bulk morphologies of these polymer−IL membranes, revealing lamellar morphology in poly(Sty-*b*-AA(MeIm)-*b*-Sty) and packed cylinders in poly(Sty-*b*-[$nBA_{4\%}$-*co*-$AA(MeIm)_{96\%}$]-*b*-Sty). Poly(Sty-*b*-AA(MeIm)-*b*-Sty) exhibited lamellar morphology, thermomechanical properties, and noteworthy ionic conductivity upon [EMIm][OTf] incorporation and proved suitable as an electromechanical actuator, with a fabricated transducer demonstrating initial response time and bending

DOI: 10.1021/acsami.5b09965
ACS Appl. Mater. Interfaces 2016, 8, 1280−1288

magnitude comparable to literature examples, even in the absence of CNC.

■ ASSOCIATED CONTENT

Supporting Information

The Supporting Information is available free of charge on the ACS Publications website at DOI: 10.1021/acsami.5b09965.

SEC data supporting the selective nature of acid hydrolysis and stability of the trithiocarbonate linkage (PDF)

■ AUTHOR INFORMATION

Corresponding Author

*E-mail: telong@vt.edu. Tel.: (540)231-2480. Fax: (540)231-8517.

Notes

The authors declare no competing financial interest.

■ ACKNOWLEDGMENTS

This material is based on work supported by the U.S. Army Research Office under Grant W911NF-07-1-0452 Ionic Liquids in Electro-Active Devices (ILEAD) MURI. The authors acknowledge the staff and facilities of the Virginia Tech Nanoscale Characterization and Fabrication Laboratory (NCFL).

■ REFERENCES

(1) Duncan, A. J.; Leo, D. J.; Long, T. E. Beyond Nafion: Charged Macromolecules Tailored for Performance as Ionic Polymer Transducers. *Macromolecules* **2008**, *41* (21), 7765−7775.
(2) Lodge, T. P. A Unique Platform for Materials Design. *Science* **2008**, *321* (5885), 50−51.
(3) Akle, B. J.; Donald, J. L. Characterization and Modeling of Extensional and Bending Actuation in Ionomeric Polymer Transducers. *Smart Mater. Struct.* **2007**, *16* (4), 1348.
(4) Akle, B. J.; Bennett, M. D.; Leo, D. J.; Wiles, K. B.; McGrath, J. E. Direct Assembly Process: A Novel Fabrication Technique for Large Strain Ionic Polymer Transducers. *J. Mater. Sci.* **2007**, *42* (16), 7031−7041.
(5) Pelrine, R.; Kornbluh, R.; Pei, Q.; Joseph, J. High-Speed Electrically Actuated Elastomers with Strain Greater Than 100%. *Science* **2000**, *287* (5454), 836−839.
(6) Gu, Y.; Cussler, E. L.; Lodge, T. P. ABA-Triblock Copolymer Ion Gels for CO2 Separation Applications. *J. Membr. Sci.* **2012**, *423−424* (0), 20−26.
(7) Wu, T.; Wang, D.; Zhang, M.; Heflin, J. R.; Moore, R. B.; Long, T. E. RAFT Synthesis of ABA Triblock Copolymers as Ionic Liquid-Containing Electroactive Membranes. *ACS Appl. Mater. Interfaces* **2012**, *4* (12), 6552−6559.
(8) Weber, R. L.; Ye, Y.; Schmitt, A. L.; Banik, S. M.; Elabd, Y. A.; Mahanthappa, M. K. Effect of Nanoscale Morphology on the Conductivity of Polymerized Ionic Liquid Block Copolymers. *Macromolecules* **2011**, *44* (14), 5727−5735.
(9) Ye, Y.; Choi, J.-H.; Winey, K. I.; Elabd, Y. A. Polymerized Ionic Liquid Block and Random Copolymers: Effect of Weak Microphase Separation on Ion Transport. *Macromolecules* **2012**, *45* (17), 7027−7035.
(10) Jangu, C.; Wang, J.-H. H.; Wang, D.; Sharick, S.; Heflin, J. R.; Winey, K. I.; Colby, R. H.; Long, T. E. Well-Defined Imidazolium ABA Triblock Copolymers as Ionic-Liquid-Containing Electroactive Membranes. *Macromol. Chem. Phys.* **2014**, *215* (13), 1319−1331.
(11) Cheng, S.; Beyer, F. L.; Mather, B. D.; Moore, R. B.; Long, T. E. Phosphonium-Containing ABA Triblock Copolymers: Controlled Free Radical Polymerization of Phosphonium Ionic Liquids. *Macromolecules* **2011**, *44* (16), 6509−6517.
(12) Zhang, S.; Lee, K. H.; Frisbie, C. D.; Lodge, T. P. Ionic Conductivity, Capacitance, and Viscoelastic Properties of Block Copolymer-Based Ion Gels. *Macromolecules* **2011**, *44* (4), 940−949.
(13) Imaizumi, S.; Kokubo, H.; Watanabe, M. Polymer Actuators Using Ion-Gel Electrolytes Prepared by Self-Assembly of ABA-Triblock Copolymers. *Macromolecules* **2011**, *45* (1), 401−409.
(14) He, Y.; Li, Z.; Simone, P.; Lodge, T. P. Self-Assembly of Block Copolymer Micelles in an Ionic Liquid. *J. Am. Chem. Soc.* **2006**, *128* (8), 2745−2750.
(15) Burke, S. E.; Eisenberg, A. Effect of Sodium Dodecyl Sulfate on the Morphology of Polystyrene-b-Poly(acrylic acid) Aggregates in Dioxane−Water Mixtures. *Langmuir* **2001**, *17* (26), 8341−8347.
(16) Luo, L.; Eisenberg, A. Thermodynamic Size Control of Block Copolymer Vesicles in Solution. *Langmuir* **2001**, *17* (22), 6804−6811.
(17) Shen, H.; Eisenberg, A. Block Length Dependence of Morphological Phase Diagrams of the Ternary System of PS-b-PAA/Dioxane/H2O. *Macromolecules* **2000**, *33* (7), 2561−2572.
(18) Yu, Y.; Zhang, L.; Eisenberg, A. Morphogenic Effect of Solvent on Crew-Cut Aggregates of Amphiphilic Diblock Copolymers. *Macromolecules* **1998**, *31* (4), 1144−1154.
(19) Zhang, L.; Shen, H.; Eisenberg, A. Phase Separation Behavior and Crew-Cut Micelle Formation of Polystyrene-b-poly(acrylic acid) Copolymers in Solutions. *Macromolecules* **1997**, *30* (4), 1001−1011.
(20) Zheng, L.; Chai, Y.; Liu, Y.; Zhang, P. Controlled RAFT Synthesis of Polystyrene-b-poly(acrylic acid)-b-polystyrene Block Copolymers and their Self-assembly in an Ionic Liquid [BMIM][PF6]. *e-Polym.* **2011**, *11* (1), 436−443.
(21) Lysenko, E. A.; Bronich, T. K.; Eisenberg, A.; Kabanov, V. A.; Kabanov, A. V. Block Ionomer Complexes from Polystyrene-block-polyacrylate Anions and N-Cetylpyridinium Cations. *Macromolecules* **1998**, *31* (14), 4511−4515.
(22) Green, M. D.; Choi, J.-H.; Winey, K. I.; Long, T. E. Synthesis of Imidazolium-Containing ABA Triblock Copolymers: Role of Charge Placement, Charge Density, and Ionic Liquid Incorporation. *Macromolecules* **2012**, *45* (11), 4749−4757.
(23) Green, M. D.; Wang, D.; Hemp, S. T.; Choi, J.-H.; Winey, K. I.; Heflin, J. R.; Long, T. E. Synthesis of Imidazolium ABA triblock Copolymers for Electromechanical Transducers. *Polymer* **2012**, *53* (17), 3677−3686.
(24) Gao, R.; Wang, D.; Heflin, J. R.; Long, T. E. Imidazolium Sulfonate-containing Pentablock Copolymer-Ionic Liquid Membranes for Electroactive Actuators. *J. Mater. Chem.* **2012**, *22* (27), 13473−13476.
(25) Lai, J. T.; Filla, D.; Shea, R. Functional Polymers from Novel Carboxyl-Terminated Trithiocarbonates as Highly Efficient RAFT Agents. *Macromolecules* **2002**, *35* (18), 6754−6756.
(26) Colombani, O.; Ruppel, M.; Schubert, F.; Zettl, H.; Pergushov, D. V.; Müller, A. H. E. Synthesis of Poly(n-butyl acrylate)-block-poly(acrylic acid) Diblock Copolymers by ATRP and Their Micellization in Water. *Macromolecules* **2007**, *40* (12), 4338−4350.
(27) Li, Q.; Hu, X.; Bai, R. Synthesis of Photodegradable Polystyrene with Trithiocarbonate as Linkages. *Macromol. Rapid Commun.* **2015**, *36* (20), 1810−1815.
(28) de Freitas, A. G. O.; Trindade, S. G.; Muraro, P. I. R.; Schmidt, V.; Satti, A. J.; Villar, M. A.; Ciolino, A. E.; Giacomelli, C. Controlled One-Pot Synthesis of Polystyrene-block-Polycaprolactone Copolymers by Simultaneous RAFT and ROP. *Macromol. Chem. Phys.* **2013**, *214* (20), 2336−2344.
(29) Ahmad, N. M.; Charleux, B.; Farcet, C.; Ferguson, C. J.; Gaynor, S. G.; Hawkett, B. S.; Heatley, F.; Klumperman, B.; Konkolewicz, D.; Lovell, P. A.; Matyjaszewski, K.; Venkatesh, R. Chain Transfer to Polymer and Branching in Controlled Radical Polymerizations of n-Butyl Acrylate. *Macromol. Rapid Commun.* **2009**, *30* (23), 2002−2021.
(30) Rudy, C. E.; Fugassi, P. The Thermal Decomposition of Tertiary Butyl Acetate. *J. Phys. Colloid Chem.* **1948**, *52* (2), 357−363.
(31) Dugas, V.; Chevalier, Y. Chemical Reactions in Dense Monolayers: In Situ Thermal Cleavage of Grafted Esters for Preparation of Solid Surfaces Functionalized with Carboxylic Acids. *Langmuir* **2011**, *27* (23), 14188−14200.

DOI: 10.1021/acsami.5b09965
ACS Appl. Mater. Interfaces 2016, 8, 1280−1288

(32) Roe, R. J. *Methods of X-Ray and Neutron Scattering in Polymer Science*; Oxford University Press, 2000.
(33) Honeker, C. C.; Thomas, E. L.; Albalak, R. J.; Hajduk, D. A.; Gruner, S. M.; Capel, M. C. Perpendicular Deformation of a Near-Single-Crystal Triblock Copolymer with a Cylindrical Morphology. 1. Synchrotron SAXS. *Macromolecules* **2000**, *33* (25), 9395−9406.
(34) Chintapalli, M.; Chen, X. C.; Thelen, J. L.; Teran, A. A.; Wang, X.; Garetz, B. A.; Balsara, N. P. Effect of Grain Size on the Ionic Conductivity of a Block Copolymer Electrolyte. *Macromolecules* **2014**, *47* (15), 5424−5431.
(35) Liu, Y.; Liu, S.; Lin, J.; Wang, D.; Jain, V.; Montazami, R.; Heflin, J. R.; Li, J.; Madsen, L.; Zhang, Q. M. Ion Transport and Storage of Ionic Liquids in Ionic Polymer Conductor Network Composites. *Appl. Phys. Lett.* **2010**, *96* (22), 223503.
(36) Hou, J.; Zhang, Z.; Madsen, L. A. Cation/Anion Associations in Ionic Liquids Modulated by Hydration and Ionic Medium. *J. Phys. Chem. B* **2011**, *115* (16), 4576−4582.

DOI: 10.1021/acsami.5b09965
ACS Appl. Mater. Interfaces 2016, 8, 1280−1288